Hearing Research 459 (2025) 109205

Contents lists available at ScienceDirect

Hearing Research

journal homepage: www.elsevier.com/locate/heares

Research paper

Finite element analysis of the osseous spiral lamina's influence on inner ear fluid flow during bone conduction stimulation

Simon Kersten [a,*], Henning Taschke [b], Michael Vorländer [a]

[a] Institute for Hearing Technology and Acoustics, RWTH Aachen University, Aachen, Germany
[b] formerly at: Institute of Communication Acoustics, Ruhr University Bochum, Bochum, Germany

ARTICLE INFO

Dataset link: https://doi.org/10.5281/zenodo.14850065

Keywords:
Bone conduction
Cochlear partition
Osseous spiral lamina
Inner ear
Third window effect

ABSTRACT

Recent studies have investigated the anatomy and motion of the human cochlear partition, revealing insights into the flexible nature of the osseous spiral lamina (OSL). These investigations have primarily focused on air-conducted stimulation, leaving the impact of the OSL's flexibility during bone-conducted (BC) stimulation largely unexplored. By considering the OSL as either flexible or rigid in a finite element model of the human inner ear, we examined the effect of the OSL's flexibility on the fluid flow in the inner ear during BC stimulation, which was divided into contributors entering via the oval window (OW) and rigid body stimulation.

Our results with rigid body stimulation indicate that the OSL facilitates an increased differential fluid flow at the round window compared to the OW, aligning with experimental observations interpreted as third window effects. Analysis of the OSL motion showed that this contribution results from a compressional motion of the OSL's vestibular and tympanic plates which is significantly lower in magnitude than the plates' translation in the direction of the stimulation. Separately applying OW input and rigid body stimulation provided insights into the interaction of BC sound entering via the OW and the reaction of the stapes to complex interior sound pressure distributions. Combined with the observations from a prior study (Kersten et al., 2024b) our results suggest a more important role for the OSL in BC hearing than previously understood. These findings enhance our understanding of the inner ear's response during BC and contribute to ongoing investigations into the interaction of BC mechanisms, while highlighting the need for further research into the deformation of the cochlear boundaries.

1. Introduction

Recent studies have investigated the anatomy and motion of the human cochlear partition (CP), challenging the classical view that its medial part, the osseous spiral lamina (OSL), is rigid. The OSL, which consists of two thin, porous plates – the vestibular plate (VP) and the tympanic plate (TP) – enveloping soft tissue and auditory nerves (Raufer et al., 2020; Bom Braga et al., 2023), has been shown to move considerably due to sound entering the inner ear (von Békésy, 1960; Stenfelt et al., 2003; Raufer et al., 2019). Additionally, the cochlear partition bridge (CPB), a soft tissue structure that connects the OSL laterally to the basilar membrane (BM), has been identified (Raufer et al., 2019).

Using a finite element model of the human inner ear, we found that the flexibility of the OSL and the presence of the CPB significantly affect the differential impedance across the CP and the related cochlear input impedance at the oval window (OW), as well as the local stiffness of the CP (Kersten et al., 2024b). The CP's influence on the cochlear sound pressure and the motion of the OSL at its lateral edge result

Abbreviations: CP, cochlear partition; OSL, osseous spiral lamina; VP, vestibular plate; TP, tympanic plate; CPB, cochlear partition bridge; BM, basilar membrane; AC, air-conducted/air conduction; BC, bone-conducted/bone conduction; OW, oval window; RW, round window; SV, scala vestibuli; ST, scala tympani; SL, spiral ligament; γ_{ow}, differential velocity between the stapes footplate and the adjacent bone, normalized to the velocity of the bone; v_{stap}, v_{prom}, measured velocities of the stapes footplate and cochlear promontory; v_{ow} (**x**), velocity of the stapes footplate in inward direction at position **x** on the OW surface; $\langle p \rangle_{ow}$, sound pressure averaged over the OW surface; $Z_{me'}$, reverse middle ear impedance; A_{ow}, area of the OW; $\mathbf{v}_{bc}$, stimulation velocity vector; $\mathbf{n}(\mathbf{x})$, unit vector perpendicular to a fluid surface in outward direction from the fluid; q_{ow}, v_{rw}, q_{osl}, q_{vp}, q_{tp}, total volume velocities associated with the OW, RW, OSL, VP, and TP; $q_{ow,diff}$, $q_{rw,diff}$, $q_{osl,diff}$, $q_{vp,diff}$, $q_{tp,diff}$, differential volume velocities associated with the OW, RW, OSL, VP, and TP; $\mathbf{v}(\mathbf{x})$, acoustic particle velocity vector at position **x**

* Corresponding author.
E-mail address: simon.kersten@akustik.rwth-aachen.de (S. Kersten).

https://doi.org/10.1016/j.heares.2025.109205
Received 18 July 2024; Received in revised form 21 January 2025; Accepted 30 January 2025
Available online 11 February 2025

in frequency- and position-dependent differences in the characteristics of the BM traveling wave, aligning with characteristics apparent in experimental data on CP motion (Gundersen et al., 1978; Stenfelt et al., 2003; Raufer et al., 2019).

However, these investigations have primarily focused on air-conducted (AC) stimulation, where sound enters the inner ear via the OW while the inner's ears surroundings remain fixed. In contrast, during bone-conducted (BC) stimulation, the inner ear's response is a result of the complex interaction of multiple mechanisms and contributions (Tonndorf, 1966, 1968; Stenfelt and Goode, 2005). Unlike AC stimulation, BC sound enters the inner ear via the OW and via vibrational stimulation of the cochlear surroundings. This vibrational input induces inertial forces within the cochlear fluid and pressure responses to cochlear bone deformation (Tonndorf, 1962; Stenfelt, 2015; Dobrev et al., 2023), both of which depend on the impedances of the two windows and the CP (Tonndorf, 1966). Additional observations, such as an unequal fluid flow between the OW and round window (RW) (Stenfelt et al., 2004) and sound transmission through the vestibular and cochlear aqueducts (Freeman et al., 2000; Sohmer and Freeman, 2004; Dobrev et al., 2022), have been regarded as "third window" mechanisms in BC hearing.

Despite these advances, the impact of the OSL's flexibility during BC stimulation has only received little attention. Tonndorf (1966) highlighted the importance of the CP impedance alongside the OW and RW impedances in influencing fluid inertial effects. Stenfelt et al. (2003) investigated BM and OSL motion in temporal bone specimens, reporting that OSL motion during BC is driven by inertial forces in the cochlear fluid and can influence intracochlear sound pressures. They acknowledged the challenge in predicting the effect of OSL motion and hypothesized that its impact on BC hearing might be significant at higher frequencies but is likely insignificant in healthy ears. Consequently, three-dimensional inner ear models used to investigate BC hearing – including BM traveling waves and the comparisons to AC (Kim et al., 2011; Ren et al., 2021; Lim et al., 2022), directional sensitivity (Kim et al., 2014), and responses to BC hearing aids (Lim et al., 2022) – have typically treated the OSL as rigid.

This paper extends previous findings on the effect of the OSL's flexibility, focusing on its impact on cochlear fluid dynamics during BC stimulation, as captured by the volume velocities at the OW and RW (Stenfelt et al., 2004) and intracochlear sound pressures (Stieger et al., 2018). In line with our previous study, we analyze the role of the OSL by modeling it either as flexible or rigid structure in our finite element model (Fig. 1). We specifically investigate two stimulation conditions (see Fig. 1, left): (1) BC sound entering the inner ear exclusively via the OW, and (2) rigid body motion of the inner ear's surroundings in a direction aligned with the OW. During the rigid body stimulation, we account for the middle ear solely as a passive load, without sound entering through the OW. In both scenarios, cochlear bone deformation – apart from the OSL – and outlets beyond the OW and RW are excluded. By capturing the fluid dynamics in the inner ear separately for these two conditions, we aim to gain deeper insights into the contribution of OSL's flexibility to BC hearing and the interaction of related mechanisms.

2. Methods

2.1. Finite element model

The inner ear model used in this study is identical to the one employed for AC stimulation in Kersten et al. (2024b). The geometry of the model was originally created as part of the work by Taschke (2005) using a dataset of an inner ear, which included grayscale images from serial sections of a temporal bone specimen with a slice thickness of 20 μm (cf. Taschke, 2005, p. 36). Contours of the scalae, vestibule, and semicircular canals were segmented in the slices and reconstructed to a three-dimensional model. Uncertainties related to the unknown post-mortem time, specimen conservation, and partial structural damage caused by slicing were mitigated by integrating prior anatomical knowledge (Gray and Lewis, 1918; Anson and Donaldson, 1981), as described in Taschke (2005, Section 4.2). More recently, we refined the original geometry to incorporate more detailed anatomical information (Cohen et al., 2005; Li et al., 2007; Atturo et al., 2014b,a; Wright and Roland, 2018; Agrawal et al., 2018; Raufer et al., 2019, 2020; Bom Braga et al., 2023). These adjustments included enhancements at the helicotrema, cochlear base, RW, OSL, and CPB.

The geometry of the inner ear and its CP are depicted in Fig. 1. Fluid domains (blue) include the vestibule, semicircular canals, scala vestibuli (SV), and scala tympani (ST). The CP separates the two scalae, with the CPB (red) and BM (purple) surfaces connecting the OSL (orange/green) with the spiral ligament (SL, brown). The SL was considered as solid domain, shell physics was assigned to the RW (olive), CPB, and BM. The entire geometry, except for the two windows, is embedded in a surrounding block of solid material (not shown in Fig. 1).

We maintained the same set of material parameters as in the prior study (Kersten et al., 2024b, Table 1). These parameters were derived from experimental sources and other models where possible, and reasonable values were assumed where no references were available. Specifically, longitudinal and radial CP coordinates were used for the implementation of inhomogeneity and anisotropy of material properties. The chosen parameters generally led to satisfactory agreements with experimental data for AC stimulation as detailed in Kersten et al. (2024b).

The OSL was modeled as a sandwich-like structure, with the VP and TP (green in Fig. 1) represented as two thin solid plates separated by a solid core (orange) with soft tissue properties. In real ears, small, randomly distributed bony pillars connect the VP and TP (Raufer et al., 2019; Bom Braga et al., 2023). This feature was approximated by connecting the plates along their lateral edge. Additionally, the OSL is semi-permeable, with varying porosity of the VP and TP depending on lateral and longitudinal position and differing across specimens (Bom Braga et al., 2023). Incorporating these complexities directly into the model was infeasible due to the high modeling complexity and limited available data. Therefore, material properties were assigned to approximate these characteristics, achieving satisfactory correspondence with AC stimulation data (Kersten et al., 2024b). However, the results should be interpreted in the light of this simplified representation of OSL.

In contrast to our previous study, we did not observe a significant impact on the results when the CPB was modeled as either flexible or rigid, provided the OSL remained rigid. Therefore, we only present results for cases where only the OSL was either flexible or rigid, while the CPB remained flexible.

2.2. BC contributors entering via the OW

Two stimulation conditions were investigated. First, to relate the BC contributions entering the inner ear via the OW to the vibration of the cochlear bone, we adopted an approach similar to that of Stenfelt (2016, 2020). This approach utilized a measured differential velocity between the stapes footplate and the adjacent bone, normalized to the velocity of the bone:

$$\gamma_{\mathrm{ow}} = \frac{v_{\mathrm{stap}} - v_{\mathrm{prom}}}{v_{\mathrm{prom}}} = \frac{v_{\mathrm{stap}}}{v_{\mathrm{prom}}} - 1\,, \tag{1}$$

where v_{stap} is the velocity of the stapes footplate, and v_{prom} is the velocity of the cochlear bone, both measured in the same direction (Stenfelt et al., 2002). In Stenfelt (2016, 2020), γ_{ow} was multiplied by the area of the stapes footplate to define the OW volume velocity as an input to a lumped element model of the inner ear, characterizing the BC sound that enters the inner ear via the middle ear. For this study, we directly

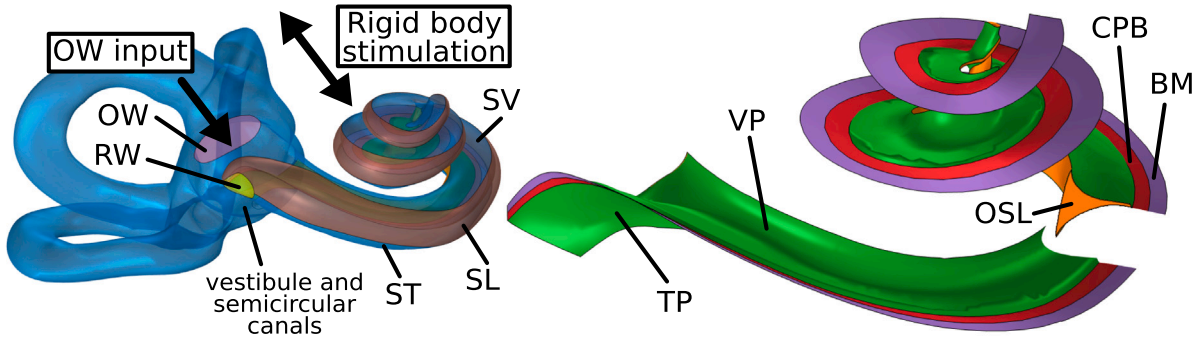

Fig. 1. Geometry of the inner ear model and its CP. Arrows represent the two stimulation conditions: input at the OW and rigid body motion of the surrounding structures, both directed perpendicular to the OW. The CP is depicted with a cutout to display its cross-section, illustrating that the VP and TP (green), the CPB (red), and the BM (purple) are included as boundary surfaces assigned with shell physics. The OSL's interior domain is highlighted in orange.

applied γ_{ow} as the input velocity at the OW, accounting for these BC contributors while the surroundings remained fixed. To obtain γ_{ow}, we subtracted 1 from the complex-valued average data for $v_{\mathrm{stap}}/v_{\mathrm{prom}}$ measured across 26 temporal bone specimens with intact middle ears reported in Stenfelt et al. (2002, Fig. 3a).

In experimental setups, separating BC sound entering via the OW from the response to inner ear motion is not feasible. Using the measured differential velocity to predict the response to BC contributors entering via the OW, as similarly done by Stenfelt (2016), implicitly assumes that these contributors were the dominant source of differential stapes motion compared to internal sound pressure acting on the stapes footplate in the average experimental data from Stenfelt et al. (2002).

For implementation, rather than directly applying γ_{ow} as velocity boundary condition at the OW, we leveraged the linearity of the model. This enabled us to scale the simulation results obtained with a unit inward velocity of 1 m/s by γ_{ow} during post-processing, remaining with the identical OW boundary condition in the finite element simulations as in Kersten et al. (2024b).

2.3. Rigid body stimulation

Second, rigid body motion was applied as a unit velocity vector of 1 m/s to the structures surrounding the inner ear (Kim et al., 2011, 2014). This approach captures the fluid inertia BC mechanism and the pressure release at the two windows (Tonndorf, 1968), while excluding the effects of cochlear bone deformation (see Section 4 for potential impacts on the results). Experimental studies (Zhao et al., 2021) and numerical simulations (Kim et al., 2014) have demonstrated the directional sensitivity of the inner ear to BC stimulation. To align with the experimental Stenfelt et al. (2004), the stimulation direction was set perpendicular to the OW. In a subset of the simulations, the OSL was modeled as rigid by also applying rigid body motion to this structure. By normalizing the amplitude of the stimulation velocity vector to unity, the results for OW input and rigid body stimulation could be directly compared, as both were referenced to the same quantity.

During the rigid body stimulation, a lumped model of the reverse middle ear impedance $Z_{\mathrm{me}\prime}$ was applied at the OW, derived from experimental data during RW stimulation by dividing SV pressure through OW volume velocity (Frear et al., 2018). $Z_{\mathrm{me}\prime}$ was modeled as a series resonator with parameters $R_{\mathrm{me}\prime} = 4.76 \times 10^{10}\,\mathrm{Pas/m^3}$, $L_{\mathrm{me}\prime} = 7.78 \times 10^{5}\,\mathrm{Pas^2/m^3}$, and $C_{\mathrm{me}\prime} = 2.56 \times 10^{-15}\,\mathrm{Pa/m^3}$ (Frear et al., 2018). In the finite element model, the impedance boundary condition at the OW was implemented as a velocity condition:

$$v_{\mathrm{ow}}(\mathbf{x}) = -\left[\frac{\langle p\rangle_{\mathrm{ow}}}{Z_{\mathrm{me}\prime} \times A_{\mathrm{ow}}} + \mathbf{v}_{\mathrm{bc}} \cdot \mathbf{n}(\mathbf{x})\right], \tag{2}$$

where $v_{\mathrm{ow}}(\mathbf{x})$ represents the inward acoustic particle velocity at positions $\mathbf{x}$ on the OW surface, and $\langle p\rangle_{\mathrm{ow}}$ the surface-averaged sound pressure at the OW (equal to the force acting on the stapes footplate divided by the OW area, A_{ow}). The dot product $\mathbf{v}_{\mathrm{bc}} \cdot \mathbf{n}(\mathbf{x})$ captures the local normal component of the stimulation velocity vector $\mathbf{v}_{\mathrm{bc}}$, calculated using the unit vector $\mathbf{n}(\mathbf{x})$ perpendicular to the surface in outward direction from the fluid.

To illustrate Eq. (2), consider a scenario where the inner ear's surroundings are fixed in position (i.e., $\mathbf{v}_{\mathrm{bc}} = \mathbf{0}$). In this case, Eq. (2) reduces to the classical impedance equation for $Z_{\mathrm{me}\prime}$, consistent with its measurement during RW stimulation (Frear et al., 2018) and its use in previous BC studies (Stenfelt, 2015, 2016; Guan et al., 2020; Ren et al., 2021). However, during BC stimulation, the temporal bone structures adjacent to the OW are in motion, necessitating the inclusion of this velocity in the impedance boundary condition.[1] This is highlighted, for example, at a frequency where $Z_{\mathrm{me}\prime}$ is acoustically rigid. In this case, Eq. (2) simplifies to $v_{\mathrm{ow}}(\mathbf{x}) \approx -\mathbf{v}_{\mathrm{bc}} \cdot \mathbf{n}(\mathbf{x})$, indicating that the stapes footplate moves with the adjacent bone (the negative sign reflects inward versus outward velocity definitions). Omitting $\mathbf{v}_{\mathrm{bc}}$ would incorrectly imply that $v_{\mathrm{ow}}(\mathbf{x}) = 0$, suggesting that the OW surface remains fixed in position despite the motion of the inner ear.

Thus, this OW boundary condition conceptually incorporates the middle ear as part of the moving system, preserving the acoustic reaction to lymph pressure at the OW while excluding BC contributors entering the inner ear via the OW.

2.4. Volume velocities

Two types of volume velocities were evaluated, illustrated in Fig. 2. *Total volume velocities* q_{ow}, q_{rw}, q_{vp} and q_{tp} were calculated by integrating the normal component of the acoustic particle velocity vector $\mathbf{v}$ over the surfaces in contact with the fluid:

$$q_k = \iint_{S_k} \mathbf{v}(\mathbf{x}) \cdot \mathbf{n}(\mathbf{x})\,\mathrm{d}S \quad k \in \{\mathrm{rw}, \mathrm{ow}, \mathrm{vp}, \mathrm{tp}\}\ . \tag{3}$$

Here, S_k represents the surface, and $\mathbf{v}(\mathbf{x}) \cdot \mathbf{n}(\mathbf{x})$ is the normal component of the acoustic particle velocity in outward direction of the fluid at a position $\mathbf{x}$ on the surface. *Differential volume velocities* $q_{\mathrm{ow,diff}}$, $q_{\mathrm{rw,diff}}$, $q_{\mathrm{vp,diff}}$ and $q_{\mathrm{tp,diff}}$ were determined by integrating the normal component of the differential velocity between the acoustic particle velocity $\mathbf{v}$ and the stimulation velocity $\mathbf{v}_{\mathrm{bc}}$:

$$q_{k,\mathrm{diff}} = \iint_{S_k} \left[\mathbf{v}(\mathbf{x}) - \mathbf{v}_{\mathrm{bc}}\right] \cdot \mathbf{n}(\mathbf{x})\,\mathrm{d}S \quad k \in \{\mathrm{rw}, \mathrm{ow}, \mathrm{vp}, \mathrm{tp}\}\ . \tag{4}$$

This calculation method for differential volume velocities is comparable to the experimental approach of Stenfelt et al. (2004) for the OW

[1] Interested readers are referred to Marburg and Anderssohn (2011) for general considerations on impedance boundary conditions in fluid–structure coupling problems, and to Kersten et al. (2024a) for related implications on prediction of the sound pressure in the ear canal.

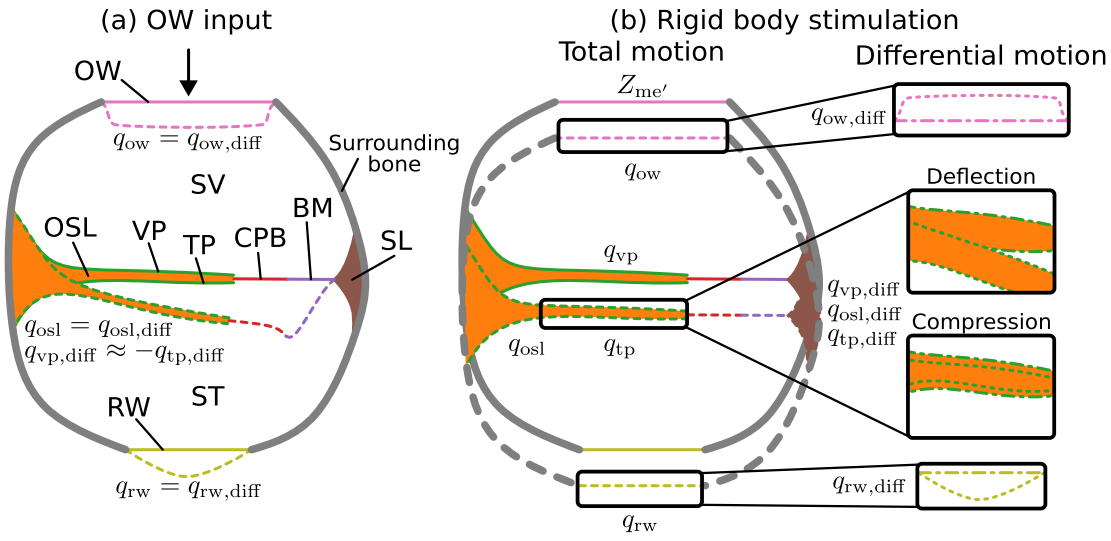

Fig. 2. Schematic cross-sectional illustration of the motion types of the OW, RW, and OSL for (a) OW input and (b) rigid body stimulation. For rigid body stimulation, the total motion (long dashed lines) is described by the total volume velocities q_{ow}, q_{rw}, q_{vp} and q_{tp}, while the differential motion components (short dashed lines) are defined relative to the translational motion (dash-dotted lines) and quantified by $q_{ow,diff}$, $q_{rw,diff}$, $q_{vp,diff}$, and $q_{tp,diff}$. OSL volume velocities are calculated as $q_{osl} = q_{vp} + q_{tp}$ and $q_{osl,diff} = q_{vp,diff} + q_{tp,diff}$. For the OSL, the two distinct types comprising the differential motion are shown: deflection, which arises from the pressure difference between the VP and TP, and compression, which results from common pressure in SV and ST. For OW input, total and differential motion are identical.

and RW, though here the integrations were performed numerically.

The total volume velocities quantify the overall motion of surfaces, while the OW and RW differential volume velocities allow for comparison with AC stimulation [cf. Stenfelt et al. (2004)]. Since the OSL surface in contact with the fluid comprises the VP and TP, the OSL volume velocities are calculated as $q_{osl} = q_{vp} + q_{tp}$ and $q_{osl,diff} = q_{vp,diff} + q_{tp,diff}$. It is important to note that, because the unit vector $\mathbf{n}(\mathbf{x})$ points outward from the inner ear, a zero-phase condition of the volume velocities defined in Eqs. (3) and (4) corresponds to fluid flow in the outward direction.

To illustrate, consider AC stimulation where $\mathbf{v}_{bc} = \mathbf{0}$. In this case, total and differential volume velocities are identical, as surface deformation is solely due to fluid pressure loading on the boundaries or, at the OW, due to the stimulation condition itself [Fig. 2(a)]. For rigid body stimulation applied to the inner ear's surroundings, the total motion of fluid surfaces coupled to structures not directly assigned the stimulation velocity – namely, the OW, RW, CP, and SL – includes both translation induced by the stimulation and deformation caused by sound pressure loading [Fig. 2(b)]. In this case, the differential volume velocities are solely governed by the sound pressure acting on the surfaces and represent the deformation relative to the translational motion. In addition, since the cochlear fluid is nearly incompressible, mass conservation ensures that the sum of the differential volume velocities across all cochlear boundaries equals zero.

The RW and OSL responses to sound pressure are implicitly handled by the fluid–structure interaction in the model, consistent with real ears. For the OW, using $v_{ow}(\mathbf{x}) = -\mathbf{v}(\mathbf{x}) \cdot \mathbf{n}(\mathbf{x})$ and substituting Eq. (2) into Eq. (4) yields:

$$q_{ow,diff} = \frac{\langle p \rangle_{ow}}{Z_{me'}}, \tag{5}$$

demonstrating that $q_{ow,diff}$ results of the sound pressure acting on the reverse middle ear impedance.

As illustrated in Fig. 2, the differential motion of the OSL comprises two distinct types: deflection and compression. Deflection arises from the pressure difference between the SV and ST or from inertial effects of the OSL, while compression is driven by the common pressure within the SV and ST. For OW input, deflection is expected to dominate, resulting in $q_{vp,diff} \approx -q_{tp,diff}$. Conversely, when compression is the primary mode of motion, $q_{vp,diff} \approx q_{tp,diff}$. These effects will be further discussed based on the simulation results.

2.5. Intracochlear sound pressure

Consistent with our previous study (Kersten et al., 2024b), intracochlear sound pressures in the SV and ST were assessed using virtual sound probes within the fluid domains. This method follows experimental setups from prior studies (Olson, 1998; Nakajima et al., 2009; Frear et al., 2018; Stieger et al., 2018; Borgers et al., 2019; Dobrev et al., 2022). Additionally, following Eq. (5), the average sound pressure over the OW surface, $\langle p \rangle_{ow}$, was evaluated.

2.6. Simulation parameters and post-processing

The simulations were conducted using Comsol Multiphysics® version 6.2, covering frequencies from 100 Hz to 10 kHz with a resolution of 12 frequencies per octave. The meshing parameters were kept as in Kersten et al. (2024b).

The volume velocities and sound pressures were exported in .csv format and analyzed using custom Python scripts. The updated version of the finite element model including the rigid body stimulation, the simulation results, and Python code used for the analysis are provided at https://doi.org/10.5281/zenodo.14850065.

3. Results

The results are structured to systematically investigate the influence of the OSL's flexibility on inner ear fluid dynamics. First, total and differential volume velocities at the OW, RW, and OSL are presented for both stimulation conditions to characterize the types of motion occurring at these boundaries. The differential volume velocity associated with the SL was found to be negligible compared to these boundaries, indicating that it behaves as a rigid structure and is therefore not discussed further. Comparisons of OW and RW differential volume velocities are made with experimental data from Stenfelt et al. (2004). Next, the individual contributions of the OSL (divided into VP and TP) and OW to the RW differential volume velocity are analyzed in more detail. Since the differential volume velocities are driven by sound pressure loading, intracochlear sound pressures are subsequently examined. These include probe evaluations compared to experimental data from Stieger et al. (2018) as well as visualizations of three-dimensional sound pressure distributions.

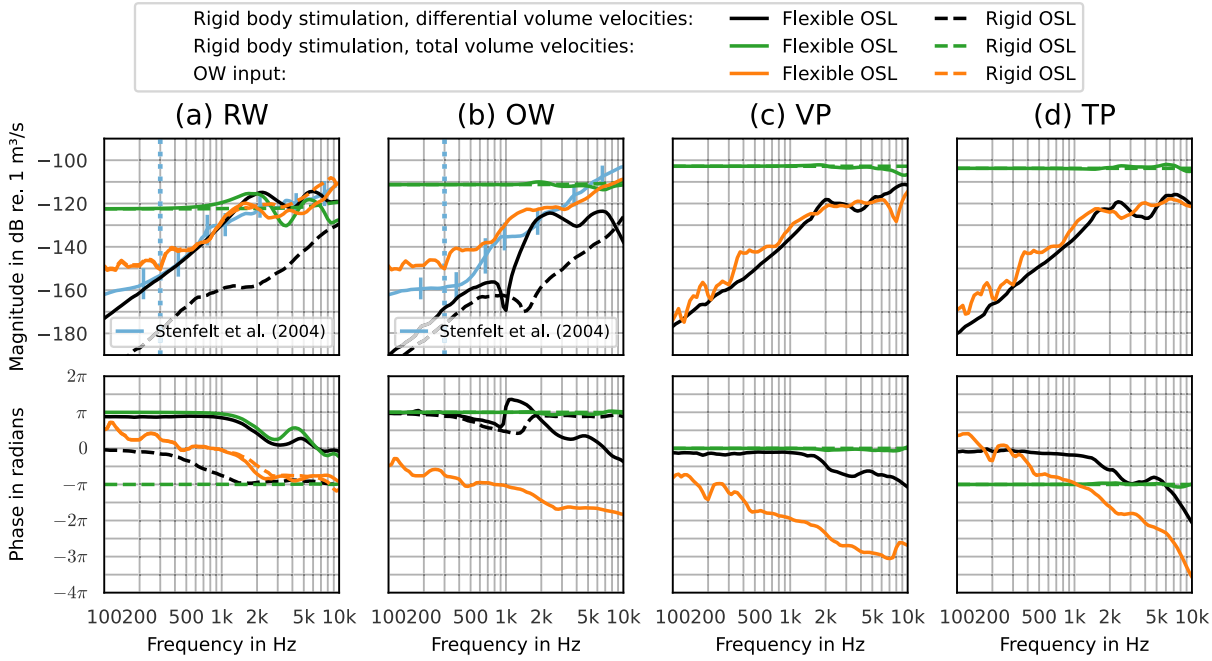

Fig. 3. Magnitude and phase of the volume velocities associated with the (a) RW, (b) OW, (c) VP, and (d) TP. Black lines indicate differential and green lines total volume velocities with rigid body stimulation. Orange lines represent the volume velocities for BC input at the OW, where total and differential volume velocities are identical. Solid lines represent results with flexible OSL, and dashed lines with rigid OSL. The OW and RW differential volume velocity magnitudes are compared to the experimental data from Stenfelt et al. (2004) (blue, mean and standard deviation), which were recalculated to volume velocities instead of volume displacements. The vertical dotted lines indicate the lower frequency limit (300 Hz) for the validity of the experimental data.

3.1. Volume velocities

Fig. 3 presents the total and differential volume velocities for (a) the RW, (b) the OW, (c) the VP, and (d) the TP. Black and green lines represent differential and total volume velocities, respectively, under rigid body stimulation, while orange lines correspond to BC input at the OW. As detailed in Section 2.4, the total and differential volume velocities are identical for the OW input condition. The differential volume velocity magnitudes at the OW and RW are compared against experimental data obtained by Stenfelt et al. (2004) from measurements on eight temporal bones. These experimental results were converted from volume displacements to volume velocities. In these measurements, the middle ear structures were removed, leaving only the stapes footplate and annular ligament at the OW. The BC stimulation directions were perpendicular to the stapes footplate, consistent with the rigid body stimulation direction applied in the model. The experimental data is shown as the mean ± standard deviation. According to an error analysis in Stenfelt et al. (2004), these results are considered valid above approximately 300 Hz, as indicated by the vertical dotted lines.

3.1.1. General observations

The magnitudes of the differential volume velocities under rigid body stimulation with a flexible OSL (solid black lines) exhibit similar trends for the surfaces in Fig. 3(a)–(d). These curves increase with a slope of approximately 40 dB per decade up to about 1 kHz, followed by alternating behavior around constant values above 2 kHz. For the OW, VP, and TP [Fig. 3(b)–(d)], the total volume velocity magnitudes under rigid body stimulation (green lines) remain nearly constant with frequency and are similar for both the flexible and rigid OSL conditions. The differential volume velocity magnitudes in these cases are at least 10–20 dB lower than the total volume velocities, indicating that surface deformation due to sound pressure loading is minor compared to the rigid body motion along with the inner ear surroundings. The phases of the total velocities at either zero or $\pm\pi$ indicate whether the spatial angle between the stimulation and the average surface normals in outward direction from the fluid is within 90° or exceeds this range.

3.1.2. RW volume velocities

A significant impact of the OSL's flexibility is visible for the RW volume velocities in Fig. 3(a). The differential and total volume velocities under rigid body stimulation with flexible OSL (solid black and green lines) show similar magnitudes above approximately 1 kHz, indicating comparable contributions of rigid body motion and deformation due to sound pressure loading on the RW in this frequency range. The RW differential volume velocities under both rigid body stimulation and OW input (solid black and orange lines) align with the experimental data from Stenfelt et al. (2004) within the standard deviation.

In contrast, under rigid body stimulation with a rigid OSL (dashed black line), the RW differential volume velocities are 30–40 dB lower than those for the flexible OSL up to 2 kHz. Above this frequency, the difference between the conditions reduces to 10 dB towards 10 kHz due to a continuous increase for the rigid OSL condition. Additionally, except between approximately 500 Hz and 2 kHz the differential velocity results with flexible versus rigid OSL show phase differences close to π, indicating opposite directions of RW motion relative to the rigid body stimulation. As a result, the total velocity curves with flexible OSL alternate with frequency in a range of $\pm$10 dB around the constant value of the rigid OSL condition above 1 kHz.

For OW input (orange lines), RW volume velocities match the experimental magnitudes above approximately 400 Hz, and the differential volume velocities for rigid body stimulation and flexible OSL above 500 Hz. The impact of OSL flexibility is limited to a reduction of approximately 5 dB in magnitude above 2 kHz.

3.1.3. OW differential volume velocity

The OW differential volume velocity under rigid body stimulation (solid black line) exhibits a distinct notch near 1 kHz [Fig. 3(b)]. This minimum corresponds to a minimum in the sound pressure distribution, as further inspected in Section 3.3. Similarly, the rigid OSL condition (dashed black line) shows a notch at approximately 1.5 kHz.

The flexible OSL condition exhibits higher magnitudes between 1 kHz and 8 kHz, with a maximum difference of approximately 35 dB around 2 kHz. Below 800 Hz, both conditions show similar phase and

increase with a 40 dB per decade slope, though the magnitudes with flexible OSL are about 5 dB higher.

The experimental data (blue lines) aligns with the simulation results for a flexible OSL within standard deviation between approximately 300–500 Hz and 1.5–3 kHz. Above 3 kHz, the simulation results are 10–35 dB lower than the experimental data. For the rigid OSL condition (dashed black line), the difference from the experimental values is at least 20 dB above 1 kHz.

Since the OW volume velocity is the input for the corresponding OW stimulation condition (orange), the OW differential volume velocities are equal for the two OSL conditions. These results align with the experimental data above approximately 500 Hz.

3.1.4. VP and TP volume velocities

The VP and TP volume velocities [Fig. 3(c)–(d)] show that the deformation of these structures is small compared to their overall motion for both the BC input at the OW (orange) and the rigid body stimulation (black). The phase difference of π between the VP and TP total volume velocities (green) reflects their opposing positions on the OSL, though both move in the same direction [see Fig. 2].

3.2. Differential volume velocities referenced to the RW

From Fig. 3 it is difficult to directly relate the differential volume velocities to each other. Since the RW impedance is significantly lower than the reverse middle ear impedance at the OW (Frear et al., 2018), differential fluid flow from both the OW and within the inner ear is predominantly directed toward the RW (Stenfelt et al., 2004). To facilitate comparison, Fig. 4 presents the differential volume velocities normalized to the RW differential volume velocity for (a) OW input and (b) rigid body stimulation. Solid lines indicate the ratios $q_{\mathrm{ow,diff}}/q_{\mathrm{rw,diff}}$ (black), $q_{\mathrm{osl,diff}}/q_{\mathrm{rw,diff}}$ (orange), $q_{\mathrm{vp,diff}}/q_{\mathrm{rw,diff}}$ (green), and $q_{\mathrm{tp,diff}}/q_{\mathrm{rw,diff}}$ (red) for a flexible OSL. The dashed black lines represent $q_{\mathrm{ow,diff}}/q_{\mathrm{rw,diff}}$ with a rigid OSL, while all other ratios are zero ($-\infty$ dB) for this condition. By normalizing to the RW outlet, the OW results can directly be compared to experimental data from Stenfelt et al. (2004, Fig. 6 and 10). The experimental magnitudes, corresponding to AC and BC stimulation in the original study, are shown in blue, including both mean curves and individual data.

3.2.1. OW input

For BC input at the OW [Fig. 4(a)], the magnitude of $q_{\mathrm{ow,diff}}/q_{\mathrm{rw,diff}}$ (black lines) remains within 3 dB up to approximately 2 kHz independent of the OSL condition. Along with the phases at $\pm\pi$, this indicates that the inward fluid flow at the OW is nearly equal to the outward flow, consistent with the experimental data for AC stimulation reported by Stenfelt et al. (2004). Between 2 kHz and 8 kHz, the simulation results with a flexible OSL show an increase of up to 8 dB, whereas the rigid OSL results align more closely with the experimental data, typically within 5 dB.

The VP and TP ratios (green and red lines) exhibit similar magnitudes below approximately 1 kHz, with a phase difference of π. This indicates that the VP and TP volume velocities largely cancel each other out. As sketched in Fig. 2(a), this cancellation results from their synchronous motion driven by the differential cochlear pressure acting on the OSL (Raufer et al., 2019; Kersten et al., 2024b). This synchronous motion leads to a differential OSL volume velocity (orange line) that is approximately 20–35 dB lower than the RW differential volume velocity in this frequency range. Above 2 kHz, the phase difference between the VP and TP curves diverges from π, indicating that the synchronous motion is partially superimposed by a deformation that varies between the VP and TP. This leads to an increase of the OSL volume velocity with a slope of 60 dB per decade between 1–2 kHz, reaching values within 5 dB of the RW differential volume velocity between 2–8 kHz.

3.2.2. Rigid body stimulation

For rigid body stimulation [Fig. 4(b)], the RW differential volume velocity closely matches that of the OSL, as indicated by the orange line remaining near 0 dB in magnitude and zero in phase throughout the entire frequency range. This suggests that the RW differential volume velocity originates primarily from the OSL, which differs fundamentally from the case of OW input.

The VP and TP contributions (green and red lines) remain between −10 dB and 0 dB up to approximately 7 kHz, with a phase close to zero. This indicates a predominantly compressional differential motion of the OSL rather than deflection [Fig. 2(b)], such that the VP and TP contribute constructively to the overall OSL volume velocity without significant cancellation. Fig. 3(c) and (d) show that this compressional motion component is at least 10–20 dB lower than the translational motion component, with differences of up to 80 dB at low frequencies.

The OW differential volume velocity with flexible OSL (solid black line) is 10–20 dB lower than the RW differential volume velocity for rigid body stimulation. The notch at about 1 kHz from Fig. 3(b) – related to a pressure minimum inspected in more detail in Section 3.3 – reappears in Fig. 4(b). In contrast, with rigid OSL (dashed black lines), the RW and OW differential volume velocities are nearly equal in magnitude and phase, except for the notch at 1.5 kHz.

The experimental OW-to-RW differential volume velocity ratio reported by Stenfelt et al. (2004) ranges between −5 dB and −10 dB on average from 400 Hz–2 kHz, with values increasing up to 10 dB toward 10 kHz. These differences between the OW and RW differential fluid flow are less pronounced than those observed in the simulations with flexible OSL, reflecting the discrepancies in OW differential volume velocity between measurement and simulation results already evident in Fig. 3(b).

3.3. Intracochlear sound pressure

To further investigate how the differential volume velocities are governed by intracochlear sound pressure, Fig. 5 presents the sound pressure results in (a) the SV, and (b) the ST. Black lines indicate point probe evaluations for rigid body stimulation with flexible (solid) and rigid OSL (dashed), while green lines represent the average sound pressure over the OW surface under the same stimulation condition. Orange lines depict probe sound pressure data for BC input at OW. The point probe positions correspond to those used in our previous study on AC stimulation (Kersten et al., 2024b), consistent with experimental studies (Stieger et al., 2018; Frear et al., 2018). Experimental data from Stieger et al. (2018, Fig. 11), measured using fiberoptic sensors in SV and ST of temporal bone specimens with intact middle ears under BC excitation, are included in blue as mean curves and individual data.

For rigid body stimulation with a rigid OSL (dashed black lines), the sound pressure in both the SV (a) and ST (b) increases with a slope of approximately 20 dB per decade. This indicates that the sound pressure is driven by the inertial behavior of the cochlear fluid. With a flexible OSL (solid black lines), the sound pressures remain within 5 dB of the rigid OSL condition up to 1 kHz. Above 1 kHz, they exhibit pronounced increases, with local maxima near 2 kHz and 7 kHz, reaching comparable magnitudes in both SV and ST.

These simulation results align with the lower range of values of the experimental data range (blue) in the SV above 2 kHz and in the ST across the entire frequency range. However, in the SV at frequencies below 1 kHz, the simulation results fall approximately 10–20 dB below the experimental values. This discrepancy arises because the experimental data represent the inner ear's response to BC stimulation without distinguishing between OW input and rigid body stimulation. Indeed, the simulation results for BC input at the OW (orange lines) remain with the experimental range throughout the frequency range in both SV and ST. For this input, the OSL's flexibility reduces the SV sound pressure above approximately 500 Hz, consistent with our previous findings regarding the cochlear input impedance (Kersten et al., 2024b). The ST sound

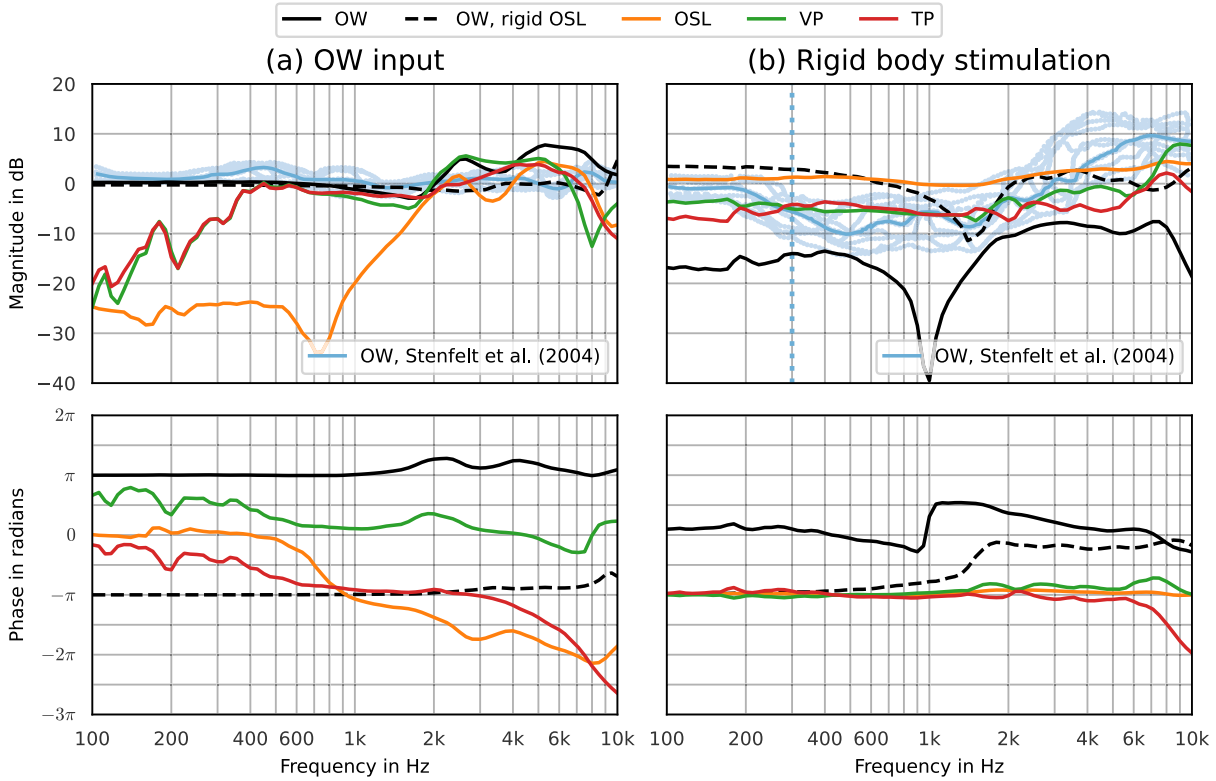

Fig. 4. Magnitude and phase of the differential volume velocity contributions to the RW differential volume velocity for (a) input at the OW with fixed surroundings and (b) rigid body stimulation in the direction of the OW. Solid lines indicate the ratios $q_{\mathrm{ow,diff}}/q_{\mathrm{rw,diff}}$ (black), $q_{\mathrm{osl,diff}}/q_{\mathrm{rw,diff}}$ (orange), $q_{\mathrm{vp,diff}}/q_{\mathrm{rw,diff}}$ (green), and $q_{\mathrm{tp,diff}}/q_{\mathrm{rw,diff}}$ (red) with flexible OSL. Dashed black lines represent $q_{\mathrm{ow,diff}}/q_{\mathrm{rw,diff}}$ with a rigid OSL, while the other ratios are zero ($-\infty$ dB) under this condition. Experimental OW magnitude ratios from Stenfelt et al. (2004) are shown in blue, corresponding to AC and BC stimulation in the original study, including individual data and mean values. The vertical dotted line indicates the lower frequency limit (300 Hz) for the validity of the experimental data in (b).

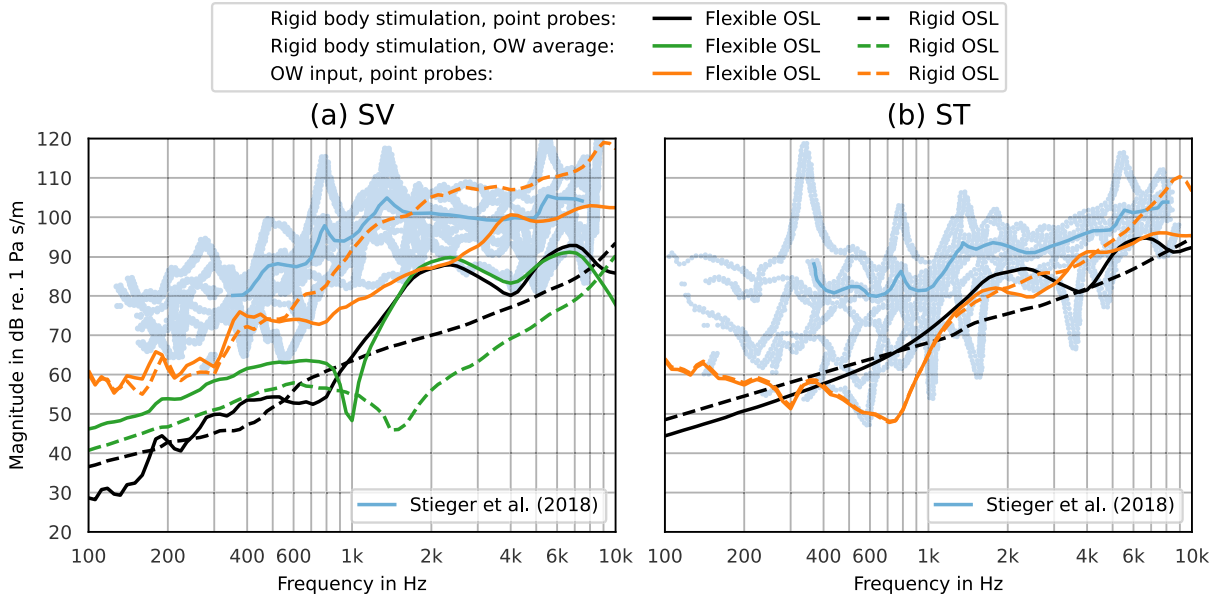

Fig. 5. Magnitude of the sound pressure in (a) the SV and (b) the ST. Black and green lines show results for the rigid body stimulation condition, evaluated using point probes and pressure averaged over the OW surface, respectively. Orange lines present the sound pressure for BC input at OW. Solid lines indicate a flexible and dashed lines a rigid OSL. Experimental data from Stieger et al. (2018), measured using fiberoptic sensors in eight temporal bone specimens with intact middle ears, is shown in blue (mean and individual data).

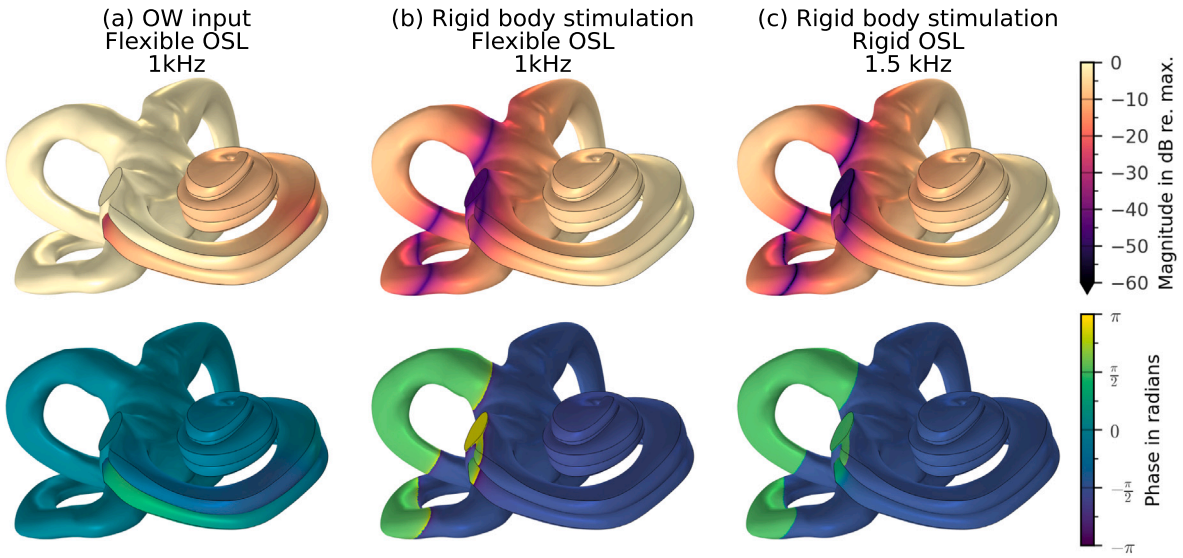

Fig. 6. Sound pressure distributions on the outer surface of the inner ear for (a) input at the OW with flexible OSL at 1 kHz, (b) rigid body stimulation and flexible OSL at 1 kHz, and (c) rigid body stimulation and rigid OSL at 1.5 kHz. Magnitudes (top row) are normalized to the maximum pressure in the inner ear, the phase data is presented relative to the stimulation velocity.

pressure is less affected, with differences attributable to local pressure variations near the cochlear base, as previously observed for the RW impedance (Kersten et al., 2024b).

The OW average pressure for rigid body stimulation with a flexible OSL (solid green line) aligns with the SV probe pressure above approximately 1.5 kHz, but it is about 10 dB higher below 800 Hz. Comparing the OW average pressure characteristics to the OW differential volume velocity in Fig. 3(b) highlights that the OW volume velocity reflects the OW sound pressure, as enforced through the OW boundary condition detailed in Section 2.3. Accordingly, the notches observed at 1 kHz (flexible OSL) and 1.5 kHz (rigid OSL) in the volume velocity data Fig. 3(b) reappear in the OW average pressure in Fig. 5(a). Differences between OW average and probe pressures further illustrate the position dependence of the sound pressure under rigid body stimulation.

Fig. 6 depicts the intracochlear pressure distributions for rigid body stimulation with flexible OSL in (b) and rigid OSL in (c). These correspond to the notch frequencies in Figs. 3(b) and 5(a). The pressure magnitudes (top row) are normalized to the respective intracochlear maximum.

For comparison, Fig. 6(a) shows the pressure distribution for OW input with flexible OSL at 1 kHz. In this case, the sound pressure is highest in the vestibule and basal part of the SV, showing a spatially uniform magnitude and phase distribution in this portion of the inner ear. The lowest pressure occurs near the RW, about 10–20 dB below the maximum, consistent with experimental ratios (Stieger et al., 2018, Fig. 12). Near the best frequency position, the sound pressure varies between SV and ST before converging to a constant value towards the apex [right in Fig. 6(a)].

For rigid body stimulation shown in Fig. 6(b) and (c), pressure minima form on planes perpendicular to the stimulation direction. The tangential alignments of these planes with the RW correspond to the notches in OW differential volume velocity and average pressure [Figs. 3(b), 5(a)]. The level differences between minima and maxima range from 30–60 dB, much greater than for OW input. The phase data (bottom row) reveal a π phase difference across these minima. Additionally, an inspection of the fluid particle velocity distribution (results not shown here) confirmed that the fluid motion largely follows the applied rigid body stimulation, as already observed in Fig. 3.

Animations of these pressure distributions across frequencies are available in the research data for this article at https://doi.org/10.5281/zenodo.14850065. These animations show that with rigid OSL, the plane of minimum pressure perpendicular to the stimulation direction persist up to about 6 kHz, with slight frequency-dependent shifts in its position relative to the OW. With flexible OSL, similar patterns appear up to approximately 1.1 kHz, after which the distribution alternates between uniform and complex patterns, occasionally forming a minimum plane.

4. Discussion

As emphasized in our previous study (Kersten et al., 2024b), the numerical model of the inner ear should be viewed as a representation of an individual specimen rather than as a predictive model for average data. Its primary aim is to assess mechanisms and identify distinct phenomena related to the flexibility of the OSL, with the understanding that the magnitudes of these effects and related quantities will naturally vary between individual ears. Additionally, a model-based approach necessarily simplifies the complex anatomy and physiology of the inner ear, especially of the OSL, so the results may not reflect all aspects of real-world behavior in precise detail. The complexity of assessing the inner ear's response to BC stimulation arises from the multiple pathways through which sound reaches the cochlea (Tonndorf, 1966, 1968; Stenfelt and Goode, 2005). To address this, we separated the mechanisms between (1) contributions that enter the inner ear via the OW, modeled by applying measured average OW input while keeping the surroundings fixed (see Section 2.2), and (2) the fluid dynamics induced by rigid body motion of the surrounding structures (see Section 2.3). Our investigations focussed on the fluid flow within the inner ear, assessed either by total volume velocities, reflecting the motion of the OW, RW and OSL surfaces, or by differential volume velocities, which capture the relative motion of these surfaces due to sound pressure loading. To enhance understanding, we also examined the relationship between volume velocities and intracochlear sound pressures, evaluating sound pressure in the SV and ST as well as spatial pressure distributions.

4.1. Total and differential motion of the OSL

A critical factor in evaluating the model predictions is recognizing the fundamentally different mechanisms driving OSL motion for OW input compared to rigid body motion of the inner ear's surroundings. For AC stimulation and BC contributors entering via the OW, the OSL

reacts to the pressure difference between the SV and ST (Fig. 6). This differential pressure leads to similar deflections of the VP and TP (schematic in Fig. 2), resulting in a significant cancellation of their respective volume velocities [Fig. 4(a)]. These findings are consistent with measurements by Raufer et al. (2019), who reported a bending of the OSL similar to a plate hinged at the medial side. Our previous simulations with AC stimulation (Kersten et al., 2024b) demonstrated behavior consistent with these experimental observations.

In contrast, during rigid body stimulation, the OSL's motion involves two components: (1) translational motion with the inner ear's surroundings, and (2) deformation caused by fluid pressure induced by the stimulation. For rigid body stimulation, we observed that the sound pressures on both sides of the OSL are – in contrast to OW input – nearly equal (Fig. 6). This results in a slight compression of the OSL [illustrated in Fig. 2(b)]. While only this compressional component contributes to the differential volume velocity, its magnitude is substantially smaller than that of the translational motion. This is evident from the differences of 20–80 dB between the VP and TP total and differential volume velocities below 4 kHz (Fig. 3). Consequently, the VP and TP move largely synchronously during rigid body stimulation, which may explain why a differential volume velocity contribution of the OSL has not yet been recognized.

Thus, understanding the OSL's contribution to fluid flow in the inner ear under BC stimulation requires separately analyzing the motions of the VP and TP. Unfortunately, there is currently no experimental data available on these motions or for the OSL's volume velocity contribution. Experimentally assessing these effects poses significant challenges. The 20–80 dB differences between VP and TP total and differential volume velocities [Fig. 3(c) and (d)] provide an estimate of the signal-to-noise ratio needed to capture differential motion of the OSL (cf. Eq. (3) and Eq. (4)). This dynamic range exceeds the capabilities of most current measurement methods. Additionally, high-resolution measurements of velocity distributions in both radial and longitudinal directions of the CP, separately for the VP and TP, would be necessary. These considerations highlight the significant experimental limitations that currently impede direct verification of the OSL's contribution to the fluid flow during BC stimulation, motivating our model-based approach.

4.2. Volume velocity contribution of the OSL

The equality in volume velocity between the OW and RW observed for OW input in Fig. 4(a) resembles experimental findings for AC stimulation (Kringlebotn, 1995; Stenfelt et al., 2004). It results from the incompressibility of the fluid and the rigid boundaries of the inner ear, where an inward flow at the OW generates an equal outward flow at the RW (Stenfelt et al., 2004; Frear et al., 2018).

In contrast, under BC stimulation, Stenfelt et al. (2004) observed unequal volume velocities at the OW and RW in temporal bone specimens where middle ear structures, aside from the stapes footplate, had been removed. At frequencies below 4 kHz, this inequality was later attributed to "third window" effects in healthy ears, referring to fluid leakage through small channels or compliant structures within the cochlea (Stenfelt and Goode, 2005). Notably, these studies did not specifically mention the OSL as one of the compliant structures when discussing this phenomenon.

Although our model excluded openings other than the OW and RW, simulations with rigid body stimulation and flexible OSL produced differences in both magnitude and phase between the differential volume velocities at the two windows [Fig. 4(b)], which are phenomenologically consistent with the experimental observations by Stenfelt et al. (2004). The simulations further demonstrated a 0 dB ratio between the OSL and RW differential volume velocities [Fig. 4(b)], identifying the flexible OSL as the dominant contributor to RW volume velocity for the rigid body stimulation condition. In contrast, with a rigid OSL, the OW-to-RW volume velocity ratio remained near 0 dB, indicating equal differential fluid flow at both windows, similar to AC stimulation. These results suggest that the flexible OSL likely contributed to the experimentally measured inequality between OW and RW volume velocities below 4 kHz.

Above 4 kHz, Stenfelt et al. (2004) observed larger differential volume velocities at the OW than at the RW, a phenomenon primarily attributed to deformations of the surrounding bone (Stenfelt and Goode, 2005). Since our rigid body stimulation excluded such deformations, this limitation likely explains the discrepancies in the OW-to-RW volume velocity ratios at higher frequencies compared to the experimental results [Fig. 4(b)].

Despite these differences in the volume velocity ratios, the quantitative agreement between the simulated and measured RW differential volume velocities [Fig. 3(a)] is noteworthy, particularly given the substantial 30–40 dB increase due to OSL flexibility compared to the rigid OSL condition. This suggests that the magnitude discrepancies in the OW-to-RW volume velocity ratio below 4 kHz may primarily stem from differences in the OW differential volume velocities when compared to the measurements by Stenfelt et al. (2004).

4.3. OW volume velocities and intracochlear sound pressure

By separating BC stimulation into input at the OW and rigid body stimulation, our approach highlights two distinct mechanisms contributing to the OW differential volume velocity during BC: (1) sound pressure acting on the stapes footplate as a reaction to inner ear motion, and (2) differential stapes motion due to BC sound originating from the middle ear or ear canal.

For rigid body stimulation, the total volume velocities [Fig. 3(b)] indicate that the OW surface primarily moves synchronously with the adjacent structures. The differential volume velocity, in this case, is exclusively driven by intracochlear pressure acting against the reverse middle ear impedance [Eq. (5)]. This behavior is confirmed by the agreement between the characteristics of OW average pressure and OW differential volume velocity curves [Fig. 5(a) and Fig. 3(b)]. A notable difference between the simulation results and experimental data is the appearance of a notch in the OW differential volume velocity for rigid body stimulation [Fig. 3(b)]. This feature arises from pressure distribution patterns with a plane of minimum pressure normal to the stimulation direction (Fig. 6). The position of this minimum plane varies slightly with frequency (cf. animations at https://doi.org/10.5281/zenodo.14850065) and aligns with the OW at approximately 1 kHz with flexible OSL and 1.5 kHz with rigid OSL. These variations, along with the disappearance of the pressure minimum in certain frequency ranges, can be attributed to the motion of the OSL, which modifies the pressure boundary conditions in the part of the inner ear comprising the SV and ST. Above approximately 1 kHz, the flexibility of the OSL increases the magnitude of both the OW average pressure and the OW differential volume velocity [Figs. 5 and 3(b)].

For BC input at the OW, the OSL's flexibility does not influence the OW differential volume velocity by definition. The differential stapes motion used as input data for this stimulation condition (Section 2.2) was derived from measurements with intact middle and inner ears (Stenfelt et al., 2002). Following Stenfelt (2016), we assumed that the contributors entering via the OW dominate this measured differential motion. However, in these experiments, BC sound transmission from the middle ear and the reaction to intracochlear pressure were inseparable, so this input data may already contain an unknown contribution from the inner ear fluid pressure.

Up to 20 dB higher magnitudes were observed in the sound pressure probe evaluations in our simulation results for OW input compared to the rigid body stimulation (Section 3.3). This reflects how a small differential motion of the stapes footplate during OW input can generate a significantly higher pressure in the cochlear fluid than the pressure caused by the rigid body motion of the inner ear driving the stapes footplate from the inside. However, since the corresponding pressure

distributions are uniquely different (Fig. 6), the relationship of these pressure components is location dependent.

When comparing the simulated pressure results with experimental data, it is important to consider that the vibration directions for intracochlear sound pressure measurements vary across specimens and fluctuate with frequency (Stieger et al., 2018; Dobrev et al., 2023), resulting in significant experimental variability [e.g., Stieger et al. (2018), Borgers et al. (2019), Dobrev et al. (2023)]. Even in temporal bone measurements with well-controlled primary stimulation directions (Stenfelt et al., 2003, 2004), stimulation velocity ratios of 3–10 (equivalent to 10–20 dB) were reported (Stenfelt et al., 2003). Consequently, the pressure ranges of 30–60 dB and corresponding notches observed in our simulations with strictly unidirectional excitation may appear less distinct in experiments due to additional pressure contributions from other directions. These considerations help explain why the simulated sound pressures for rigid body stimulation fall at the lower end – or below – the experimental values at the probe locations, while simulations for BC input at the OW remain within the experimental range (Fig. 5).

It is also important to note that the experimental reference for OW differential volume velocity under BC stimulation was obtained after removal of the malleus, incus, and portions of the stapes (Stenfelt et al., 2004), likely altering the mechanical impedance at the OW compared to intact ears. Additionally, sound pressure induced by inner ear deformation – excluded in our simulations – may have influenced the OW differential volume velocity, particularly above 4 kHz (Stenfelt and Goode, 2005). Considering these complexities, it is plausible that the experimental OW differential volume velocity magnitudes lie between our simulated results for OW input and rigid body stimulation below 3 kHz [Fig. 3(b)].

4.4. Role of the OSL in BC hearing

The role of OSL motion has received limited attention in studies of BC hearing mechanisms. Stenfelt et al. (2003) investigated BM and OSL motion under AC and BC stimulation, identifying relative motion between the OSL and the inner ear's surroundings. They concluded that the effect of OSL motion on BC hearing – termed "inertial OSL BC sound" – may contribute at higher frequencies but is likely not significant in healthy ears. However, our findings suggest a more substantial role for the flexible OSL in BC hearing. Firstly, the impact of the OSL on BC hearing should be considered in light of our earlier findings for BC sound entering via the OW. These results demonstrated that the OSL's flexibility affects the differential sound pressure and contributes an additional motion component to BM motion (Kersten et al., 2024b). Secondly, in this study, we observed a significant contribution of the OSL to the fluid flow in the inner ear in response to BC stimulation.

Tonndorf (1966) listed the impedance of the CP – which is significantly influenced by the OSL's flexibility (Kersten et al., 2024b) – as a factor affecting the fluid inertia effects during BC. This insight has been incorporated into lumped-element models of the inner ear (Stenfelt, 2015, 2016; Guan et al., 2020). However, our findings on the OSL's motion and volume velocity contribution suggest that the consideration of the CP via a single impedance should be revisited.

The RW, VP, and TP differential volume velocities exhibited similar magnitudes for both OW input and rigid body stimulation conditions (Fig. 3), and the relation of these mechanisms in the intracochlear sound pressure responses was highly dependent on frequency (Fig. 5) and position (Fig. 6). These findings highlight that, while the OSL likely plays a substantial role in differential fluid flow during BC stimulation, quantitatively predicting its contribution remains challenging due to the uncertain and variable interactions between the BC mechanisms in real ears.

To further clarify the OSL's role, it is crucial to distinguish the different effects that have been regarded as "third windows" in BC hearing: sound transmission from the skull interior via the vestibular and cochlear aqueducts (Freeman et al., 2000; Sohmer and Freeman, 2004; Dobrev et al., 2022), leakage during RW simulation (Stieger et al., 2013; Frear et al., 2018), and inequality in fluid flow between the OW and RW during BC stimulation (Stenfelt et al., 2004). Rosowski et al. (2018) pointed out that distinguishing the compressibility of the inner ear's content from anatomical third windows is challenging. In our study, additional openings beyond the OW and RW were excluded, yet the simulation reproduced the fluid flow inequality observed by Stenfelt et al. (2004). This result suggests that the flexibility of the OSL may play a significant role in this phenomenon. However, the contribution of anatomical third windows to this effect, to our knowledge, has not been quantified for healthy ears.

4.5. Study limitations and suggestions for future work

The limitations identified in our previous study on AC stimulation (Kersten et al., 2024b) – particularly, the use of a specific set of model parameters, the absence of active cochlear mechanisms, and the lack of representation of individual anatomical differences – are applicable to the current study, as the model remained essentially unchanged.

A key limitation specific to the current investigation is the simplified representation of the OSL. In the model, the OSL was treated as a sandwich-like solid structure, while in reality, both the VP and TP, along with the softer core, may be partially fluid-filled due to their porosity and semi-permeable nature. While the bending stiffness of the OSL – its most critical property influencing the inner ear's response to AC and BC input at the OW – is likely governed primarily by its solid properties, this modeling approach may not fully capture its compressibility, which could behave more fluid-like. Although this is unlikely to affect the identified mechanisms related to the OSL's compressibility, it may influence the magnitudes of the differential volume velocities observed during rigid body stimulation [Fig. 3(c) and (d)].

Our simulations focused on a specific direction of rigid body stimulation, aligning with the experimental conditions in Stenfelt et al. (2004). While primary rigid body motion of the inner ear has been observed in these experiments (Stenfelt et al., 2004) and cadaver head measurements (Dobrev et al., 2023), other studies highlighted the complexity related to such stimulation. Kim et al. (2014) and Zhao et al. (2021) reported directionality in the inner ear's BC response, while Dobrev et al. (2023) found no singular direction of motion in their cadaver head measurements. These findings underscore the need for future studies to incorporate multiple directions of stimulation to fully capture the OSL's effect on inner ear responses.

We also limited BC stimulation to two mechanisms, BC sound entering via the OW and rigid body stimulation, excluding deformation of the inner ear's surroundings (Tonndorf, 1962; Stenfelt, 2015; Dobrev et al., 2023). Two findings suggest the need for further investigation of compression and expansion of the inner ear. First, the differential volume velocity contribution of the OSL observed in our simulations arose from differences in VP and TP velocity distributions, but these velocities fall below current measurement thresholds. This highlights the importance of even minimal compressibilities in cochlear structures, which should be incorporated into future models. Particularly, rigid boundary conditions could be reconsidered by including structures such as the spongy bone of the modiolus and potential flexibility of the thin walls between cochlear turns [cf. Raufer et al. (2020, Fig. 2a)]. Secondly, the experimental observation of greater OW than RW differential velocities for BC stimulation above 4 kHz (Stenfelt et al., 2004) was attributed to cochlear bone deformation (Stenfelt and Goode, 2005). Our simulations could not replicate this phenomenon through either of the two stimulation conditions or the OSL's role as a "third window", supporting hypotheses that cochlear bone deformation plays an important role at higher frequencies.

Our approach of separating BC mechanisms using a finite element model of the inner ear extends previous efforts on predicting the

relative importance of BC contributors (Taschke, 2005; Stenfelt, 2016, 2020). Our simulation results contribute to these ongoing investigations into the mechanisms of BC hearing, highlighting the critical role of the OSL. For this study, we restricted the stimulation to OW input and rigid body motion. Future work could expand this approach to separate the outer and middle ear contributions and include additional mechanisms. Furthermore, integrating a flexible OSL with a middle ear model (Kim et al., 2014) or into a full head model (Lim et al., 2022) could yield deeper insights into the interaction between the BC pathways and inner ear structures.

5. Conclusions

This study investigated how the flexibility of the OSL influences the fluid flow in the inner ear during BC stimulation by modeling the OSL as either rigid or flexible structure in a finite element model of the human inner ear. Accounting for the OSL's sandwich-like anatomy enabled to separate the contributions from the vestibular and tympanic plates. Additionally, the BC stimulation was separated into two mechanisms: (1) BC contributors entering via the OW and (2) rigid body stimulation, while excluding inner ear deformation and OW input for the latter.

During rigid body stimulation, the OSL significantly contributed to the differential volume velocity at the RW, resulting in an increased differential fluid flow at the RW compared to the OW. This aligns with experimental observations previously interpreted as third window effects. Analysis of the OSL motion indicated that its contribution arises from compressional motion. However, this motion component is several orders of magnitude smaller than the motion associated with the rigid body stimulation. In contrast, under OW input, the OSL deflected consistent with previous measurements and model predictions, while the OSL's flexibility had only minor influence on the differential volume velocities at the two windows. Comparisons of the simulation results for the two types of stimulation and experimental data, where responses inherently reflect a mixture of BC mechanisms, provided insights into the interaction of BC sound entering via the OW and the stapes' reaction to complex sound pressure distributions within the inner ear.

Together with findings from our prior study on AC stimulation (Kersten et al., 2024b), these results suggest a more important role for the OSL in BC hearing than previously recognized, while highlighting the need for further research into the complex mechanical properties of the OSL and the deformation of the cochlear boundaries.

Source of funding

This work was funded by the Deutsche Forschungsgemeinschaft (DFG, German Research Foundation) – Project-ID 352015383 – SFB 1330 A4.

Declaration of AI and AI-assisted technologies in the writing process

During the preparation of this work, the authors used ChatGPT 3.5 and 4.0 to refine the English language and improve the wording of the manuscript. After using these tools, the authors reviewed and edited the content as needed, and take full responsibility for the content of the publication.

CRediT authorship contribution statement

Simon Kersten: Writing – original draft, Visualization, Methodology, Investigation, Formal analysis, Data curation, Conceptualization. **Henning Taschke:** Writing – review & editing, Methodology, Conceptualization. **Michael Vorländer:** Writing – review & editing, Supervision, Project administration, Funding acquisition, Conceptualization.

Declaration of competing interest

The authors declare that they have no known competing financial interests or personal relationships that could have appeared to influence the work reported in this paper.

Data availability

Research data for this article is available at https://doi.org/10.5281/zenodo.14850065. The repository contains the finite element model, simulation results, sound pressure animations, and a Python script with code used for the analysis.

References

Agrawal, S., Schart-Morén, N., Liu, W., Ladak, H.M., Rask-Andersen, H., Li, H., 2018. The secondary spiral lamina and its relevance in cochlear implant surgery. Upsala J. Med. Sci. 123 (1), 9–18. http://dx.doi.org/10.1080/03009734.2018.1443983.

Anson, B., Donaldson, J., 1981. Surgical Anatomy of the Temporal Bone. W.B. Saunders company, Philadelphia, London, Toronto.

Atturo, F., Barbara, M., Rask-Andersen, H., 2014a. Is the human round window really round? An anatomic study with surgical implications. Otol. Neurotol. 35 (8), 1354. http://dx.doi.org/10.1097/MAO.0000000000000332.

Atturo, F., Barbara, M., Rask-Andersen, H., 2014b. On the anatomy of the 'hook' region of the human cochlea and how it relates to cochlear implantation. Audiol. Neurotol. 19 (6), 378–385. http://dx.doi.org/10.1159/000365585.

von Békésy, G., 1960. Experiments in hearing. In: McGraw-Hill Series in Psychology, McGraw-Hill, New York.

Bom Braga, G.O., Parrilli, A., Zboray, R., Bulatović, M., Wagner, F., 2023. Quantitative evaluation of the 3D anatomy of the human osseous spiral lamina Using MicroCT. J. Assoc. Res. Otolaryngol. 24 (4), 441–452. http://dx.doi.org/10.1007/s10162-023-00904-3.

Borgers, C., Fierens, G., Putzeys, T., van Wieringen, A., Verhaert, N., 2019. Reducing artifacts in intracochlear pressure measurements to study sound transmission by bone conduction stimulation in humans. Otol. Neurotol. 40 (9), e858. http://dx.doi.org/10.1097/MAO.0000000000002394.

Cohen, D., Blinder, G., Perez, R., Raveh, D., 2005. Standardized computed tomographic imaging and dimensions of the round-window niche. Int. Tinnitus J. 11 (2), 158–162.

Dobrev, I., Farahmandi, T., Pfiffner, F., Röösli, C., 2022. Intracochlear pressure in cadaver heads under bone conduction and intracranial fluid stimulation. Hear. Res. 108506. http://dx.doi.org/10.1016/j.heares.2022.108506.

Dobrev, I., Pfiffner, F., Röösli, C., 2023. Intracochlear pressure and temporal bone motion interaction under bone conduction stimulation. Hear. Res. 435, 108818. http://dx.doi.org/10.1016/j.heares.2023.108818.

Frear, D.L., Guan, X., Stieger, C., Rosowski, J.J., Nakajima, H.H., 2018. Impedances of the inner and middle ear estimated from intracochlear sound pressures in normal human temporal bones. Hear. Res. 367, 17–31. http://dx.doi.org/10.1016/j.heares.2018.06.019.

Freeman, S., Sichel, J.-Y., Sohmer, H., 2000. Bone conduction experiments in animals – evidence for a non-osseous mechanism. Hear. Res. 146 (1), 72–80. http://dx.doi.org/10.1016/S0378-5955(00)00098-8.

Gray, H., Lewis, W.H., 1918. Anatomy of the Human Body. Lea & Febiger.

Guan, X., Cheng, Y., Galaiya, D., Rosowski, J., Lee, D., Nakajima, H., 2020. Bone-conduction hyperacusis induced by superior canal dehiscence in human: The underlying mechanism. Sci. Rep. 10 (1), http://dx.doi.org/10.1038/s41598-020-73565-4.

Gundersen, T., Skarstein, ø., Sikkeland, T., 1978. A study of the vibration of the basilar membrane in human temporal bone preparations by the use of the Mossbauer effect. Acta Oto- Laryngol. 86 (1–6), 225–232. http://dx.doi.org/10.3109/00016487809124740.

Kersten, S., Sgard, F., Vorländer, M., 2024a. Impact of the ear canal motion on the impedance boundary conditions in models of the occlusion effect. J. Acoust. Soc. Am. 155 (1), 56–67. http://dx.doi.org/10.1121/10.0024244.

Kersten, S., Taschke, H., Vorländer, M., 2024b. Influence of the cochlear partition's flexibility on the macro mechanisms in the inner ear. Hear. Res. 109127, http://dx.doi.org/10.1016/j.heares.2024.109127.

Kim, N., Homma, K., Puria, S., 2011. Inertial bone conduction: Symmetric and anti-symmetric components. J. Assoc. Res. Otolaryngol. 12 (3), 261–279. http://dx.doi.org/10.1007/s10162-011-0258-3.

Kim, N., Steele, C.R., Puria, S., 2014. The importance of the hook region of the cochlea for bone-conduction hearing. Biophys. J. 107 (1), 233–241. http://dx.doi.org/10.1016/j.bpj.2014.04.052.

Kringlebotn, M., 1995. The equality of volume displacements in the inner ear windows. J. Acoust. Soc. Am. 98 (1), 192–196. http://dx.doi.org/10.1121/1.413746.

Li, P.M.M.C., Wang, H., Northrop, C., Merchant, S.N., Nadol, J.B., 2007. Anatomy of the round window and hook region of the cochlea with implications for cochlear implantation and other endocochlear surgical procedures. Otol Neurotol 28 (5), 641–648. http://dx.doi.org/10.1097/mao.0b013e3180577949.

Lim, J., Dobrev, I., Röösli, C., Stenfelt, S., Kim, N., 2022. Development of a finite element model of a human head including auditory periphery for understanding of bone-conducted hearing. Hear. Res. 421, http://dx.doi.org/10.1016/j.heares.2021.108337.

Marburg, S., Anderssohn, R., 2011. Fluid structure interaction and admittance boundary conditions: Setup of an analytical example. J. Comp. Acous. 19 (01), 63–74. http://dx.doi.org/10.1142/S0218396X11004274.

Nakajima, H.H., Dong, W., Olson, E.S., Merchant, S.N., Ravicz, M.E., Rosowski, J.J., 2009. Differential intracochlear sound pressure measurements in normal human temporal bones. J. Assoc. Res. Otolaryngol. 10 (1), 23–36. http://dx.doi.org/10.1007/s10162-008-0150-y.

Olson, E.S., 1998. Observing middle and inner ear mechanics with novel intracochlear pressure sensors. J. Acoust. Soc. Am. 103 (6), 3445–3463. http://dx.doi.org/10.1121/1.423083.

Raufer, S., Guinan, J.J., Nakajima, H.H., 2019. Cochlear partition anatomy and motion in humans differ from the classic view of mammals. Proc. Natl. Acad. Sci. USA 116 (28), 13977–13982. http://dx.doi.org/10.1073/pnas.1900787116.

Raufer, S., Idoff, C., Zosuls, A., Marino, G., Blanke, N., Bigio, I.J., O'Malley, J.T., Burgess, B.J., Nadol, J.B., Guinan, J.J., Nakajima, H.H., 2020. Anatomy of the human osseous spiral lamina and cochlear partition bridge: Relevance for cochlear partition motion. J. Assoc. Res. Otolaryngol. 21 (2), 171–182. http://dx.doi.org/10.1007/s10162-020-00748-1.

Ren, L.J., Yu, Y., Fang, Y.Q., Hua, C., Dai, P.D., Zhang, T.Y., 2021. Finite element simulation of cochlear traveling wave under air and bone conduction hearing. Biomech. Model. Mechanobiol. 20 (4), 1251–1265. http://dx.doi.org/10.1007/s10237-021-01443-7.

Rosowski, J.J., Bowers, P., Nakajima, H.H., 2018. Limits on normal cochlear 'third' windows provided by previous investigations of additional sound paths into and out of the cat inner ear. Hear. Res. 360, 3–13. http://dx.doi.org/10.1016/j.heares.2017.11.003.

Sohmer, H., Freeman, S., 2004. Further evidence for a fluid pathway during bone conduction auditory stimulation. Hear. Res. 193 (1), 105–110. http://dx.doi.org/10.1016/j.heares.2004.03.015.

Stenfelt, S., 2015. Inner ear contribution to bone conduction hearing in the human. Hear. Res. 329, 41–51. http://dx.doi.org/10.1016/j.heares.2014.12.003.

Stenfelt, S., 2016. Model predictions for bone conduction perception in the human. Hear. Res. 340, 135–143. http://dx.doi.org/10.1016/j.heares.2015.10.014.

Stenfelt, S., 2020. Investigation of mechanisms in bone conduction hyperacusis with third window pathologies based on model predictions. Front. Neurol. 11.

Stenfelt, S., Goode, R.L., 2005. Bone-conducted sound: Physiological and clinical aspects. Otol. Neurotol. 26 (6), 1245–1261. http://dx.doi.org/10.1097/01.mao.0000187236.10842.d5.

Stenfelt, S., Hato, N., Goode, R.L., 2002. Factors contributing to bone conduction: The middle ear. J. Acoust. Soc. Am. 111 (2), 947–959. http://dx.doi.org/10.1121/1.1432977.

Stenfelt, S., Hato, N., Goode, R.L., 2004. Fluid volume displacement at the oval and round windows with air and bone conduction stimulation. J. Acoust. Soc. Am. 115 (2), 797–812. http://dx.doi.org/10.1121/1.1639903.

Stenfelt, S., Puria, S., Hato, N., Goode, R.L., 2003. Basilar membrane and osseous spiral lamina motion in human cadavers with air and bone conduction stimuli. Hear. Res. 181 (1), 131–143. http://dx.doi.org/10.1016/S0378-5955(03)00183-7.

Stieger, C., Guan, X., Farahmand, R.B., Page, B.F., Merchant, J.P., Abur, D., Nakajima, H.H., 2018. Intracochlear sound pressure measurements in normal human temporal bones during bone conduction stimulation. J. Assoc. Res. Otolaryngol. 19 (5), 523–539. http://dx.doi.org/10.1007/s10162-018-00684-1.

Stieger, C., Rosowski, J.J., Nakajima, H.H., 2013. Comparison of forward (ear-canal) and reverse (round-window) sound stimulation of the cochlea. MEMRO 2012 – Middle-Ear Bridge between Science and Otology, Hear. Res. MEMRO 2012 – Middle-Ear Bridge between Science and Otology, 301, 105–114.http://dx.doi.org/10.1016/j.heares.2012.11.005,

Taschke, H., 2005. Mechanismen der Knochenschallleitung (Mechanisms of bone-conducted sound) (Ph.D. thesis). Ruhr University Bochum, Bochum, Germany, http://dx.doi.org/10.13154/294-10197.

Tonndorf, J., 1962. Compressional bone conduction in cochlear models. J. Acoust. Soc. Am. 34 (8), 1127–1131. http://dx.doi.org/10.1121/1.1918259.

Tonndorf, J., 1966. Synopsis a revised theory of bone conduction. Acta Oto- Laryngol. 61 (sup213), 7–9. http://dx.doi.org/10.3109/00016486609120796.

Tonndorf, J., 1968. A new concept of bone conduction. Arch. Otolaryngol. 87 (6), 595–600. http://dx.doi.org/10.1001/archotol.1968.00760060597008.

Wright, C.G., Roland, P.S., 2018. Anatomy of the helicotrema and cochlear apex. In: Wright, C.G., Roland, P.S. (Eds.), Cochlear Anatomy Via Microdissection with Clinical Implications: An Atlas. Springer International Publishing, Cham, pp. 27–43. http://dx.doi.org/10.1007/978-3-319-71222-2_2.

Zhao, M., Fridberger, A., Stenfelt, S., 2021. Vibration direction sensitivity of the cochlea with bone conduction stimulation in guinea pigs. Sci. Rep. 11 (1), 2855. http://dx.doi.org/10.1038/s41598-021-82268-3.